Motion of a screw dislocation in a two-dimensional Peierls potential

Keiichi Edagawa and Takayoshi Suzuki
Institute of Industrial Science, University of Tokyo, Roppongi, Minato-ku, Tokyo 106, Japan

Shin Takeuchi
Faculty of Industrial Science and Technology, Science University of Tokyo, Yamazaki, Noda, Chiba 278, Japan
(Received 1 April 1996)

Motion of a screw dislocation in a crystal lattice occurs by kink pair formation in a two-dimensional Peierls potential. Employing the line-tension model of a dislocation, the saddle-point configuration of a nonplanar kink pair in three-dimensional space and the associated activation energy are calculated. The method is applied to a $\langle 111 \rangle$ screw dislocation in a bcc lattice assuming a threefold periodic sinusoidal Peierls potential in the (111) plane. In this potential the dislocation can nucleate a kink pair from one stable straight configuration towards any of the three adjacent ones. Depending on the direction of the applied stress the relative frequencies of the three activation processes determine the temperature dependence of the critical flow stress and the direction of total slip. The calculations reproduce well the plastic anisotropy of bcc transition metals. [S0163-1829(97)02210-8]

I. INTRODUCTION

A dislocation moving in a crystal lattice feels a resistance due to lattice periodicity. The lattice resistance is usually expressed in terms of a periodic function of the position of a straight dislocation (Peierls potential[1–3]). At finite temperature and under an applied stress the mobility of the dislocation is given by the nucleation rate of kink pairs in the straight segment lying in the potential valley, provided that the migration rate of the nucleated kinks is sufficiently high.[4–11] The kink pair formation rate has usually been calculated for a certain assumed (for example, sinusoidal) shape of the potential. In any existing theory the Peierls potential is assumed to be a one-dimensional periodic function $V_P(x)$ on a specific slip plane zx, where z is the direction of the dislocation line. The saddle-point configuration of a planar bow-out $x(z)$ in the slip plane and the associated energy ΔH are calculated either in the line-tension model[4,5,7] or considering self-stresses in a bow-out configuration.[10,11] Theories of this type have been widely applied to the analysis of the low-temperature plasticity of various crystals including bcc metals[5,7,12–14] and ionic crystals.[15–17]

bcc metals, in particular at low temperature, are plastically anisotropic: they show a strong temperature dependence and shear asymmetry of slip.[13,18] Since *in situ* electron microscopy observation revealed that the deformation is controlled by the motion of screw dislocations,[19] these characteristic features should be interpreted by the properties of a screw dislocation in the bcc lattice. Of the two different models proposed for the slip behavior in bcc metals one is based on a threefold dissociation of the dislocation core,[20,21] and the other one on a threefold symmetric Peierls potential.[22] The results of atomistic calculations on the dislocation core structure, Peierls stress, and also behavior under stress[13,23] have often been interpreted as a mixing of these two effects.[23] Most of the simulations are concerned with absolute zero temperature. Takeuchi and Kuramoto[12] attempted to describe the plastic anisotropy at finite temperatures by thermally activated kink pair formation on a screw dislocation. They considered an effective Peierls potential for the transition from one stable position to another through an intermediate metastable position, calculated the nucleation rate of a kink pair along each possible path with the theory[4–7] of one-dimensional Peierls potentials and then superimposed the transition probabilities in three possible directions to obtain the dislocation velocity and resulting slip plane at a given temperature. In the calculation the activation path between two stable configurations was specified, though the path itself should be chosen so as to minimize the activation energy. Recently, Suzuki, Koizumi, and Kirchner[14] investigated the temperature dependence of the flow stress and showed that some experimental curves are apparently described by a damlike Peierls potential with a flat maximum, but others can never be reproduced by such one-dimensional potentials. These investigations suggest that the motion of screw dislocations must be treated without specifying its glide plane even on the atomistic scale. The Peierls potential of a screw dislocation must be defined as a two-dimensional function $V_P(x,y)$ in the plane (x,y) normal to the dislocation line z. The bow out is not planar any more, but the dislocation line is now a space curve on a developable surface. The saddle-point configuration of a bow out $[x(z),y(z)]$ must be found in the three-dimensional space (x,y,z) under applied stress τ to obtain the activation energy.

This paper calculates the saddle-point energy for a nonplanar bow out of a dislocation in a two-dimensional Peierls potential. The method is applied to a screw dislocation in the bcc lattice and the plastic anisotropy is derived from a simple potential which reflects merely the structural symmetry. The line-tension model is employed for the expression of the elastic energy of the bow-out configuration.

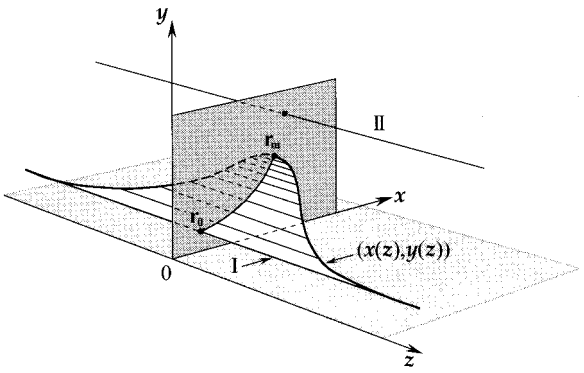

FIG. 1. Bow-out configuration $[x(z),y(z)]$ of a dislocation moving in the Peierls potential $V_P(x,y)$ from the initial equilibrium position I at $\mathbf{r}=\mathbf{r}_0$ towards the adjacent equilibrium position II. The projection of the symmetric configuration onto the xy plane is the curve $\mathbf{r}=\mathbf{r}(x,y)$ from $\mathbf{r}_0$ to $\mathbf{r}_m$.

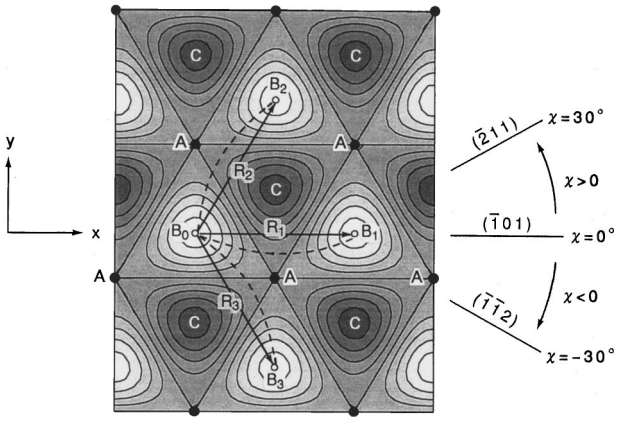

FIG. 2. Two-dimensional Peierls potential $V_P(x,y)$ for a $\langle 111\rangle$ screw dislocation in the bcc lattice, Eq. (5). The atomic rows parallel to $\langle 111\rangle$ are located at the positions A. The potential minima are at B_0, B_1, B_2, and B_3, and maxima at C. χ is the angle between the plane of the maximum shear stress τ and the (101) plane, i.e., the direction of the force τb acting on the dislocation. $\mathbf{R}_i$ is the transition vector from B_0 to B_i, $i=1$, 2, and 3. The broken line linking B_0 and B_i is the shape of an isolated kink projected on the (111) plane; see Sec. IV.

II. SADDLE-POINT CONFIGURATION AND ENERGY OF A KINK PAIR IN A TWO-DIMENSIONAL PEIERLS POTENTIAL

Figure 1 presents a schematic illustration of the thermally activated motion of a dislocation in a two-dimensional Peierls potential under a certain applied stress. We consider a dislocation along the z direction moving from a stable equilibrium position (line I) to another different stable equilibrium position adjacent to it (line II). When the effective Peierls potential, which includes the work done by the applied stress, is lower at position II than at position I, the whole dislocation could make a transition from position I to position II via a thermally activated saddle-point configuration having a bow-out shape as illustrated in Fig. 1. The thermal activation energy in this process is given by the energy increment in the saddle-point configuration with respect to the initial equilibrium configuration I. The problem is to determine the three-dimensional saddle-point configuration and to evaluate the associated energy in a given two-dimensional Peierls potential under an applied stress.

The line-tension model expresses the total-energy increment of the dislocation having the configuration $\mathbf{r}(z)=[x(z),y(z)]$ with respect to the initial equilibrium configuration at $\mathbf{r}_0=(x_0,y_0)$ as

$$E[x(z),y(z)]=\int_{-\infty}^{\infty}\left[\frac{1}{2}\Gamma\left\{\left(\frac{dx}{dz}\right)^2+\left(\frac{dy}{dz}\right)^2\right\}+\Phi(x,y)-\Phi(x_0,y_0)\right]dz, \tag{1}$$

where Γ denotes the line-tension of the dislocation and $\Phi(x,y)$ is the effective Peierls potential including the work done term, which will be given explicitly in Eq. (6). For a screw dislocation along $\langle 111\rangle$, Γ is known to be independent of the plane of the bow-out.[24] The saddle-point configuration must satisfy the Euler-Lagrange equations of the functional (1),

$$\Gamma\frac{d^2x}{dz^2}=\frac{\partial\Phi(x,y)}{\partial x},\quad \Gamma\frac{d^2y}{dz^2}=\frac{\partial\Phi(x,y)}{\partial y}. \tag{2}$$

which are just the equilibrium equations between the line-tension force and the force by the potential. The saddle-point configuration is the solution of the differential equations (2) under the boundary conditions $x(-\infty)=x(+\infty)=x_0$ and $y(-\infty)=y(+\infty)=y_0$, which are the solutions of $\partial\Phi/\partial x=0$ and $\partial\Phi/\partial y=0$, respectively.

An analogy should be pointed out between Eqs. (2) and Newton's equation of motion; by replacing the coordinate z with the time t, Eqs. (2) transform into the equation of motion of a single particle with mass Γ in the potential field $U(x,y)=-\Phi(x,y)$. In this mechanical analog the path of the particle $\mathbf{r}(t)=[x(t),y(t)]$ represents the shape of the dislocation $\mathbf{r}(z)=[x(z),y(z)]$. The saddle-point configuration of the dislocation corresponds to the following particle motion: (a) A particle placed at $\mathbf{r}_0=(x_0,y_0)$, the top of the potential $U(x,y)$, runs down the potential hill. (b) The particle subsequently climbs up a potential hill next to it to reach a point $\mathbf{r}_m=(x_m,y_m)$ with the same potential value as that at $\mathbf{r}_0=(x_0,y_0)$. (c) The particle goes back through the same path to reach the initial point $\mathbf{r}_0=(x_0,y_0)$. It is noteworthy that the particle never reaches the same potential height as that at $\mathbf{r}_0$, unless the right starting directions are chosen. However, once we find the path to reach the point with such potential height, i.e., $\mathbf{r}_m$, the particle motion (c) is ensured by the reversal invariance of the equation of motion. After all, the problem is reduced to obtaining either the forward path from $\mathbf{r}_0$ to $\mathbf{r}_m$ or the return path from $\mathbf{r}_m$ to $\mathbf{r}_0$. Assuming that electron and phonon drags are negligible throughout the above-described processes, (a)–(c), the ''mechanical energy'' should be preserved, i.e.,

$$\frac{1}{2}\Gamma\left\{\left(\frac{dx}{dz}\right)^2+\left(\frac{dy}{dz}\right)^2\right\}=\Phi(x,y)-\Phi(x_0,y_0). \tag{3}$$

By substituting Eq. (3) into Eq. (1), we obtain the saddle-point energy ΔH as

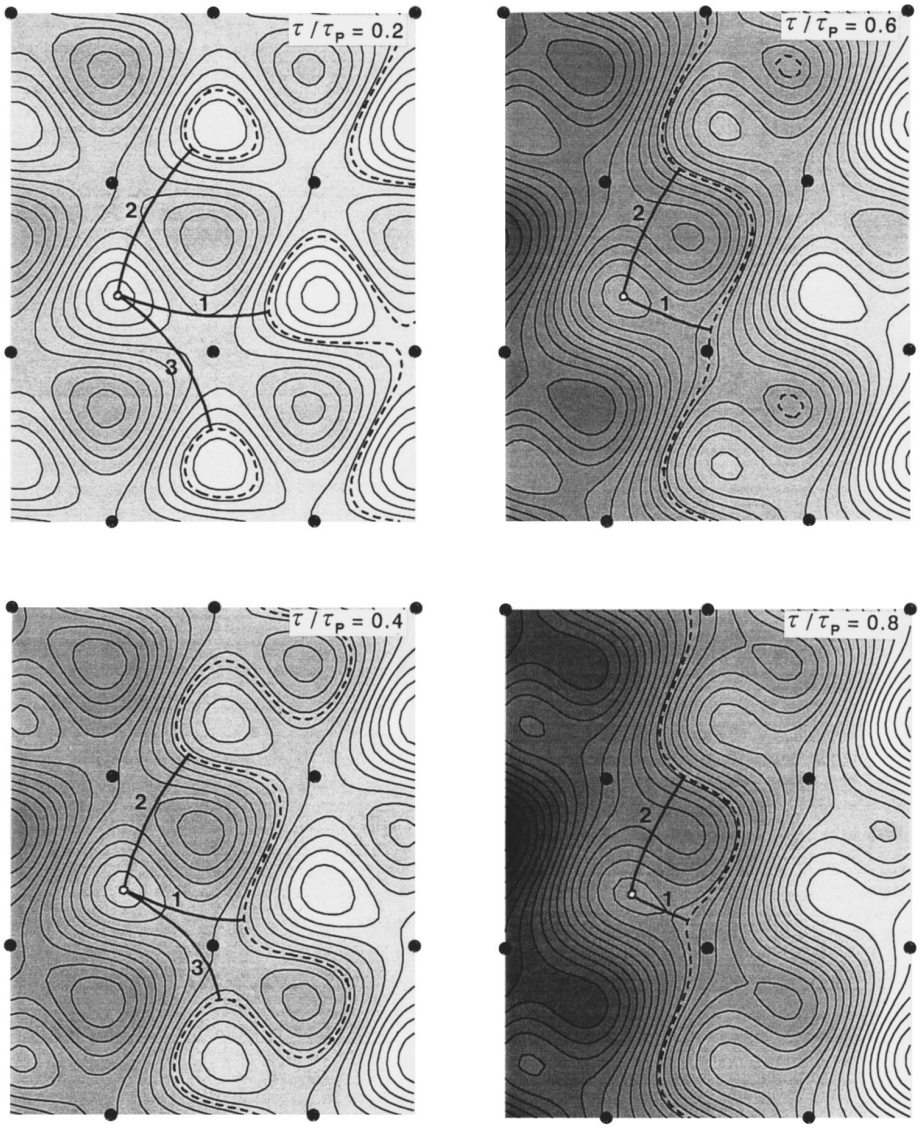

FIG. 3. Contour maps of the effective potential $\Phi(x,y;\tau)$ defined by Eq. (6) for $\chi=0°$. The Peierls stress $\tau_P(\chi=0°)$ is $3.8\times10^{-3}\mu$. A minimum position (x_0,y_0) under the stress τ is indicated by a small circle. The broken line is the contour of $\Phi(x,y)=\Phi(x_0,y_0)$. The calculated saddle-point configurations of the bow out towards three neighboring minimums are shown as the curved paths projected on the xy plane.

$$\Delta H=2\sqrt{2\Gamma}\int_{\mathbf{r}_0}^{\mathbf{r}_m}\sqrt{\Phi(x,y)-\Phi(x_0,y_0)}\;dl, \tag{4}$$

where $dl=\sqrt{dx^2+dy^2}$ denotes the line element along the path.

III. APPLICATION TO A bcc LATTICE

We consider a screw dislocation with Burgers vector $\mathbf{b}=1/2\langle111\rangle$ in the bcc lattice. The atomic rows parallel to the $\langle111\rangle$ axis form a triangular lattice with lattice parameter $a=(2\sqrt{2}/3)|\mathbf{b}|$ in the (111) plane. Hence, due to the symmetry of the lattice, low-energy positions should be aligned also in the form of the same triangular lattice. As every simulation has shown,[22,23,25] we assume that the low-energy positions are located at every other center of the triangles. We simulate this situation by assuming a sinusoidal Peierls potential

$$V_P(x,y)=\frac{8}{3\sqrt{3}}V_0\sin\frac{2\pi}{\sqrt{3}}\frac{y}{a}\sin\frac{\pi}{a}\left(\frac{y}{\sqrt{3}}+x\right)\times\sin\frac{\pi}{a}\left(\frac{y}{\sqrt{3}}-x\right), \tag{5}$$

where V_0 corresponds to $(V_P^{\max}-V_P^{\min})/2$. This two-dimensional Peierls potential is depicted in Fig. 2. We express the mode of stressing by the angle χ according to the conventional notation, where $\chi=-30°$, $0°$ and $+30°$ correspond to the shear stressing on the twinning $(\bar{1}12)$ plane, the (101) plane and the antitwinning (211) plane, respectively. The effective Peierls potential under the applied shear stress τ in the plane represented by χ can be written as

$$\Phi(x,y;\tau,\chi)=V_P(x,y)-\tau b(x\cos\chi+y\sin\chi). \tag{6}$$

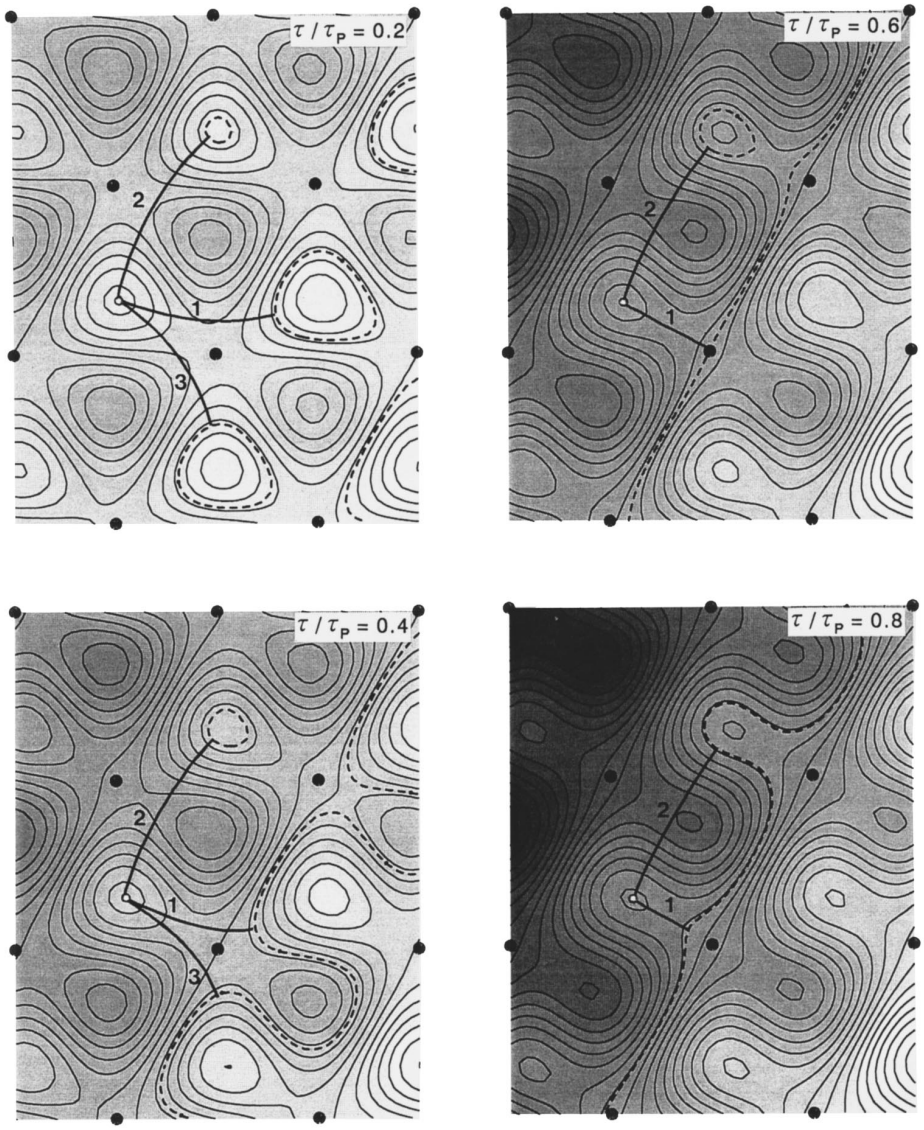

FIG. 4. Contour maps of the effective potential $\Phi(x,y;\tau)$ for $\chi=-25°$ and the saddle-point configurations of the bow-out. The Peierls stress $\tau_P(\chi=-25°)$ is $3.3\times10^{-3}\mu$.

The angle χ means now the direction of the force τb acting on the dislocation. For every χ between $-30°$ and $+30°$, the dislocation at a stable equilibrium position B_0 can make a transition to one of the three of neighboring stable positions B_1, B_2, and B_3 in Fig. 2.

For $\chi=\pm30°$, one of the three transitions is in a critical situation, in which the effective Peierls potential value for the initial position and that for the position after the transition become exactly the same. The saddle-point configuration for each transition is calculated as follows: (a) Contour lines having the value of $\Phi(x_0,y_0;\tau,\chi)$ are calculated for a given τ and χ. (b) A particle is placed at a certain point on the contour lines and its time evolution is investigated by the equation of motion for the potential $-\Phi(x,y;\tau,\chi)$. (c) By changing the initial point on the contour lines step by step, the path to reach (x_0,y_0) is searched for, which gives the saddle-point configuration of the dislocation, as explained in Sec. II. The activation energy associated with the saddle-point configuration is calculated from Eq. (4).

The frequency of the thermally activated motion of the dislocation from one stable equilibrium position to another is

$$\nu=\nu_0\ \exp\left(-\frac{\Delta H}{kT}\right), \tag{7}$$

where ν_0 is the frequency factor, ΔH is the activation energy, and kT has the usual meaning. In the present case in which there are three types of translation, the velocity vector of the dislocation is given by

$$\mathbf{v}=\sum_{i=1}^{3}\ \nu_i\mathbf{R}_i\,, \tag{8}$$

where ν_i and $\mathbf{R}_i$ ($i=1$, 2, and 3) denote the translation frequencies and the translation vectors for the three types of translation. The angle ψ between the integrated slip plane and the (101) plane is obtained as the angle between v and x axis, i.e.,

$$\psi=\sin^{-1}\frac{v_y}{|\mathbf{v}|}. \tag{9}$$

For the numerical calculations we take $b=2.8\times10^{-10}$m, $\mu b^3=2.0\times10^{-18}$ J, $\nu_0=10^{13}$ s^{-1}, $\Gamma=\mu b^2/2$, and $V_0=1.0\times10^{-3}\mu b^2$, which were determined from the

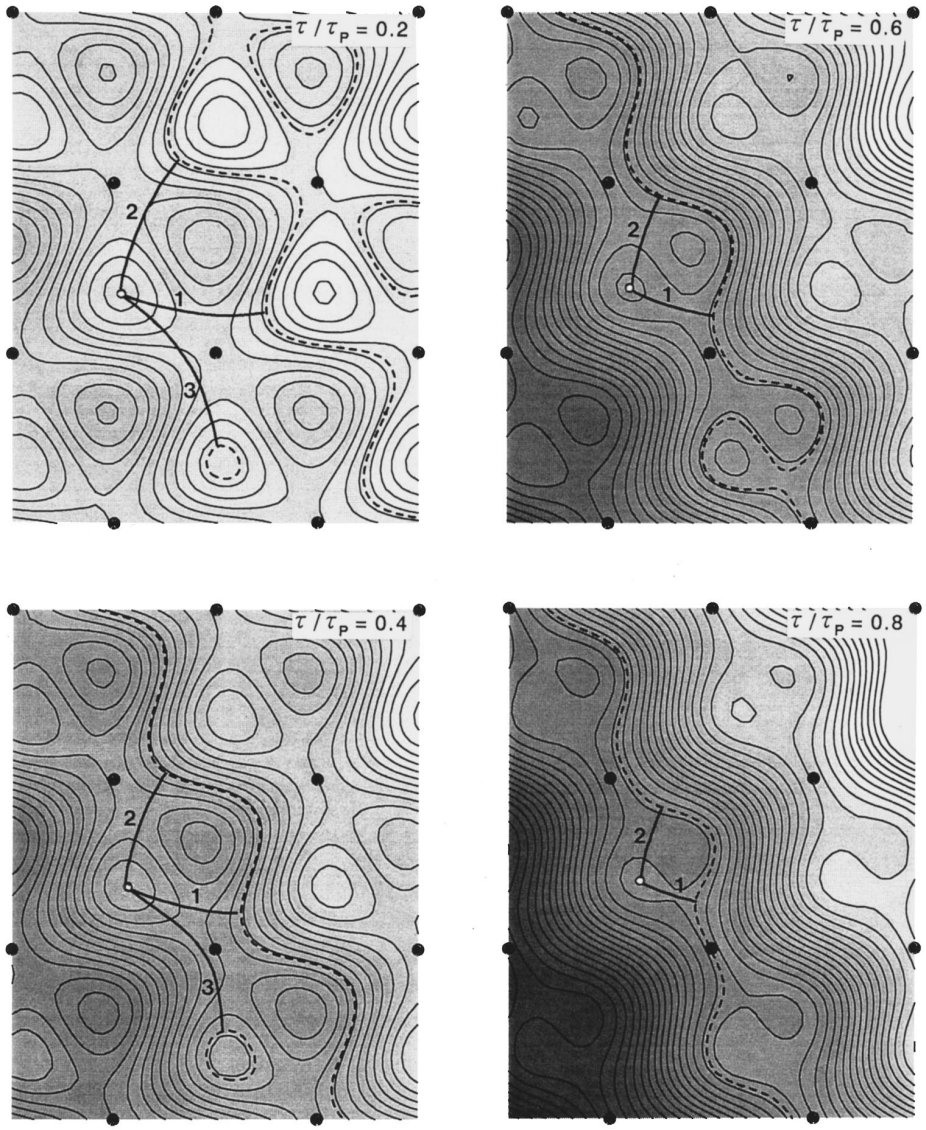

FIG. 5. The same as Figs. 3 and 4, but for $\chi=25°$. $\tau_P(\chi=25°)=5.3\times10^{-3}\mu$.

paper of Takeuchi and Kuramoto.[12] The critical velocity v_c of the dislocation at which the crystal undergoes yielding was taken as 10^{-6} m/s. With these numerical values we calculate the temperature T at which the dislocation velocity reaches v_c and the corresponding ψ at the temperature under a given stress τ and angle χ.

IV. RESULTS

Application of the force τb tilts the effective potential surface $\Phi(x,y)$ in the direction of χ, as shown in Figs. 3–5 for $\chi=-25°$, $0°$, and $25°$, respectively. When τ exceeds some critical value, the minima of Φ which are the stable positions of the dislocation vanish. This critical stress, the Peierls stress τ_P, depends on the angle χ, as will be described later (Fig. 8). The stable equilibrium position $\mathbf{r}_0=(x_0,y_0)$ of the straight configuration for a given χ and $\tau<\tau_P$ is indicated in Figs. 3–5 by open circles. With increasing τ the stable position shifts from B_0 nearly in the direction of χ. The contour lines $\Phi(x,y)=\Phi(x_0,y_0)$ are shown by broken lines in Figs. 3–5. As explained in Sec. II, the top position of the saddle-point configuration must be found on these lines. The saddle-point configurations were obtained following the procedure described in Sec. III, and their projections on the xy plane are drawn on the energy contour maps of Figs. 3–5 for respective (τ,χ) values. At $\tau=0$, all the minima at B_i in Fig. 2 are of the same energy, hence the saddle-point configuration links two neighboring minimum points, as shown by broken lines. This configuration corresponds to an isolated kink or a pair of kinks with infinite separation. It should be noted that the saddle-point configuration does not necessarily go through the saddle point of the potential $\Phi(x,y;\tau,\chi)$ itself. Also to be noted is that the translation from B_0 to B_2 or B_3 is possible only up to some limiting value of τ, though towards B_1 it is always possible. For example, the translation towards B_3 is impossible at $\tau>0.5\ \tau_P$ for any orientation. For τ close to τ_P the saddle-point configuration for the transition to B_2 also does not exist, irrespective of χ, because the contour line satisfying $\Phi(x,y;\tau,\chi)=\Phi(x_0,y_0;\tau,\chi)$ becomes almost straight; it allows only the transition to B_1.

The stress dependence of the activation energy, $\Delta H_i(\tau)$,

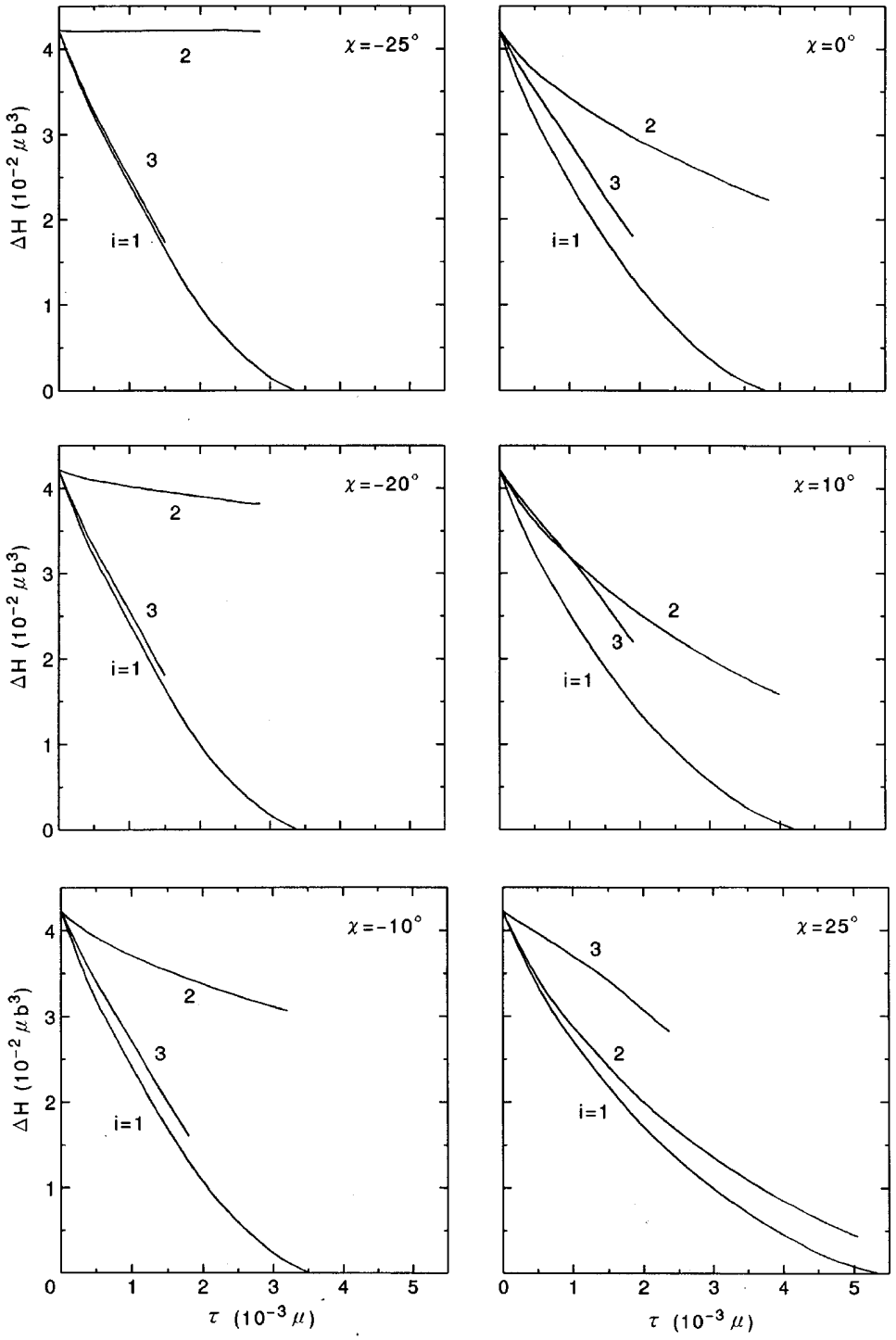

FIG. 6. Activation energy $\Delta H_i(\tau)$ for the six values of angle χ. The branches $i=1,2$, and 3 correspond to the possible transitions towards B_i identified in Fig. 2.

calculated by Eq. (4) is shown in Fig. 6, where the branch i denotes the transition from B_0 to B_i ($i=1,\ 2$, and 3) indicated in Fig. 2. The value of $\Delta H_i(\tau=0)$ is independent of both i and χ; it is equal to the energy of two isolated kinks, $2U_k$. Only $\Delta H_1(\tau)$ of the three branches covers the full stress range from $\tau=0$ to τ_P. The shape of $\Delta H_1(\tau)$ varies slowly with the angle χ according to the dependence of τ_P on χ. On the contrary, $\Delta H_2(\tau)$ and $\Delta H_3(\tau)$ change drastically with changing χ. When $\chi=-30°$, the potential surface $\Phi(x,y;\tau)$ is always symmetric with respect to the $\chi=-30°$ axis, the stress τ produces no difference between the minimum energies near B_0 and B_2, and hence $\Delta H_2(\tau)$ stays almost constant; $\Delta H_2(\tau;\chi=-30°)\approx 2U_k$. For $\chi>-30°$ the bottom of Φ near B_2 becomes deeper than that near B_0, and thus ΔH_2 reveals a τ dependence which becomes strong with increasing χ. When χ reaches $+30°$, the potential Φ becomes again symmetric with respect to the $\chi=30°$ axis, the transitions to B_1 and to B_2 become equivalent, and hence $\Delta H_2(\tau)$ coincides with $\Delta H_1(\tau)$. The curve of $\Delta H_2(\tau)$ for $\chi=25°$ in Fig. 6 is almost in this situation.

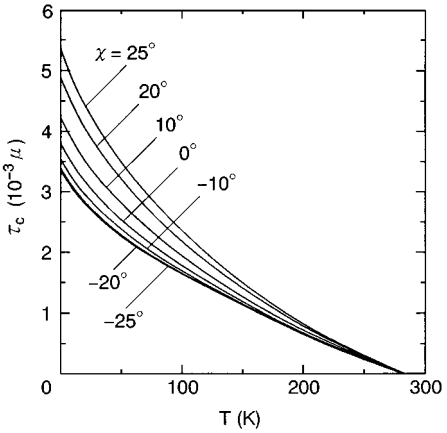

FIG. 7. Critical shear stress τ_c against temperature T for given χ.

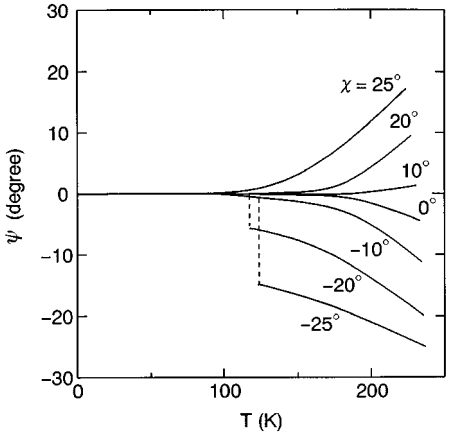

FIG. 9. Angle ψ of integrated slip plane against temperature T for given χ.

The variation of $\Delta H_3(\tau)$ with χ is in the opposite sense of $\Delta H_2(\tau)$, but not exactly so because of the asymmetry of $\Phi(x,y)$ with respect to the x axis. Corresponding to the absence of the transition paths for $i=2$ and 3 at large τ, $\Delta H_2(\tau)$ does not reach $\tau=\tau_P$ and $\Delta H_3(\tau)$ ends with τ smaller than 0.5 τ_P.

Figure 7 shows the relations between the temperature T and the stress τ_c determined so as to give $|\mathbf{v}|=v_c=10^{-6}$ m/s for Eq. (8) using the $\Delta H_i(\tau)$ curves in Fig. 6. They are equivalent to the temperature dependences of the critical shear stress observed by macroscopic deformation tests at constant strain rate, provided that the mobile dislocation density is constant. The maximum temperature $T_0\approx 280$ K below which the Peierls mechanism operates corresponds to $\Delta H_i(\tau=0)=2U_k$, and is independent of χ. The shape of $\tau_c(T)$ in Fig. 7 is dominated by $\Delta H_1(\tau)$, but the contribution of $\Delta H_2(\tau)$ and/or $\Delta H_3(\tau)$ is not small at low τ or high T, particularly for $\chi\approx\pm 30°$. The variation of τ_c with angle χ at constant T is shown in Fig. 8. The value of τ_c at $T=0$ K is the Peierls stress τ_P.

Figures 9 and 10 show the angle ψ between the integrated slip plane and the $(\overline{1}01)$ plane, which is given by Eq. (9). Referring to $\Delta H_i(\tau)$ of Fig. 6, the behavior of $\psi(T,z)$ is interpreted as follows. At low T, where the stress τ_c should be high, the velocity v of Eq. (8) is determined exclusively by ΔH_1. This means that the integrated slip plane is always the $(\overline{1}01)$ plane, i.e., $\psi=0$ irrespective of the angle χ of the applied stress, as indeed seen in Figs. 9 and 10 for $T<100$ K. On the other hand, at high T, where the stress τ_c should be low, the transition to B_2 or B_3 contributes remarkably to v and makes ψ deviate from 0° in the same sense as χ, as seen in Figs. 9 and 10 for $T>100$ K. With T increasing further, τ_c approaches zero, ΔH_2 or ΔH_3 become close to ΔH_1 (Fig. 7), and the nucleation rate of kink pairs towards B_2 or B_3 increases. Therefore, at high T the integrated slip plane becomes almost parallel to the plane of maximum shear stress, i.e., $\psi=\chi$. The discontinuities of the $\psi-T$ relations in Fig. 9 arise from the disappearance of the activation path to B_3 at large τ, seen in Figs. 4 and 6.

V. DISCUSSION

The present treatment for the kink pair formation process is based on the line-tension model of a dislocation; it assumes smooth kinks and a constant line-tension irrespective of the shape and orientation of the dislocation segment in a bow-out configuration. The line-tension model cannot be applied to the case of high Peierls potentials giving narrow or abrupt kinks, as in semiconductors. The Peierls stress of screw dislocations in bcc metals are of the order of 10^{-3} μ. This gives a kink width of about $10b$, which is

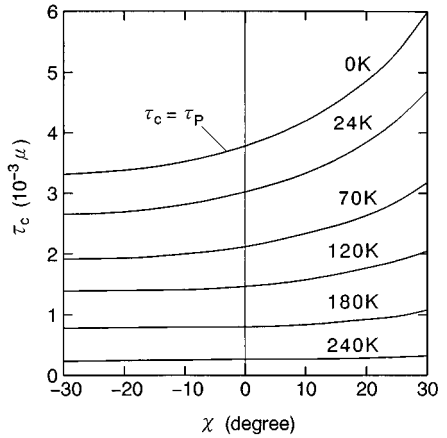

FIG. 8. $\tau_c-\chi$ relations at various temperatures.

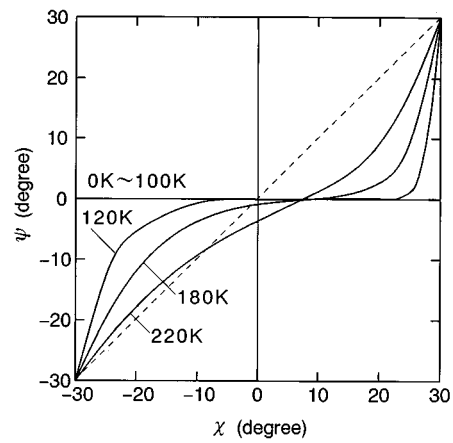

FIG. 10. $\psi-\chi$ relations at various temperatures.

wide enough to apply the line-tension model. The line-tension Γ of a screw dislocation in the bcc lattice is independent of the bow-out direction because of the threefold symmetry of the elastic field of the $\langle 111 \rangle$ dislocation.[24] Therefore, for the smooth bow-out of the dislocation into the shape of Fig. 1, the present treatment with a constant Γ is reasonable, as long as the applied stress τ is not too low. When τ is close to zero, the separation of two opposite kinks at the saddle point becomes large, so that the line-tension model loses applicability and the long-range elastic interaction (self-stress) in the bow-out should explicitly be considered to determine the saddle-point energy.[8] Recently, Koizumi, Kirchner, and Suzuki[10,11] and Suzuki, Koizumi, and Kirchner[14] investigated the kink pair formation process considering the self-stresses in the full range of applied stress τ, and showed that the line-tension model describes well the saddle-point shape of the kink pair and the stress dependence of the activation energy, except for $\tau < 0.1\tau_P$.

The present model is simple and primitive in that the assumed Peierls potential function only reflects the threefold symmetry of the screw dislocation in the bcc lattice without taking into any account the details of the bonding characteristics. In this respect, the present model is similar to the threefold symmetric dissociation model (e.g., Kroupa and Vitek[26]), which also considers only the symmetry but not the periodicity of the lattice. In spite of the simplicity of the present model, the obtained relations of $\tau_c - T$, $\tau_c - \chi$, and $\psi - \chi$ describe well the overall trends of the experiments on W,[27] Mo,[28,29] Ta,[30] Nb,[31] and α-Fe.[32] This implies that the plastic anisotropy essentially stems from the geometry or the symmetry of the screw dislocation in the bcc lattice, irrespective of the details of the core structure and also the shape of the potential. However, there are some disagreements between the present result and the experiments of α-Fe (Ref. 32) and Mo (Ref. 29) for $\chi < 0°$ and at low temperatures. In order to reproduce every detail of the particular experimental data, the potential $V_P(x,y)$ must be chosen more adequately. The calculation by use of the refined $V_P(x,y)$ is in progress and will be reported in a separate paper.

The present model assumes the energy of the dislocation to be uniquely given as a function of the position under stress. However, if it is widely spread, the energy of the dislocation may not be uniquely defined as a function of the dislocation position because the energy depends on the way of the spread. Thus, the present treatment can be applied only to a narrow core. Although the present model reproduces the experimentally well established asymmetry between forward and backward slip, it cannot explain the asymmetry between tension and compression when the hydrostatic component matters. That can only be studied by computer simulation which takes fully into account the three-dimensional relaxation of the lattice.[33]

[1] R. E. Peierls, Proc. Phys. Soc. **52**, 34 (1940).
[2] F. R. N. Nabarro, Proc. Phys. Soc. **59**, 256 (1947).
[3] F. R. N. Nabarro, *Theory of Crystal Dislocations* (Oxford University Press, Oxford, 1967), p. 139.
[4] V. Celli, M. Kabler, T. Ninomiya, and R. Thomson, Phys. Rev. **131**, 58 (1963).
[5] J. E. Dorn and S. Rajnak, Trans. AIME **230**, 1052 (1964).
[6] A. Seeger and P. Schiller, *Physical Acoustics, Principles and Methods*, edited by W. P. Mason (Academic, New York, 1966), Vol. IIIA, p. 361.
[7] P. Guyot and J. E. Dorn, Can. J. Phys. **45**, 983 (1967).
[8] A. Seeger, Z. Metallkd. **72**, 369 (1981).
[9] J. P. Hirth and J. Lothe, *Theory of Dislocations* (Wiley-Interscience, New York, 1982), p. 532.
[10] H. Koizumi, H. O. K. Kirchner, and T. Suzuki, Acta Metall. Mater. **41**, 3483 (1993).
[11] H. Koizumi, H. O. K. Kirchner, and T. Suzuki, Philos. Mag. A **69**, 805 (1994).
[12] S. Takeuchi and E. Kuramoto, J. Phys. Soc. Jpn. **38**, 480 (1975).
[13] S. Takeuchi, see Sec. 5 in T. Suzuki, S. Takeuchi, and H. Yoshinaga, *Dislocation Dynamics and Plasticity* (Springer, Berlin, 1991), p. 77.
[14] T. Suzuki, H. Koizumi, and H. O. K. Kirchner, Acta Metall. Mater. **43**, 2177 (1995).
[15] T. Suzuki and H. Kim, J. Phys. Soc. Jpn. **39**, 1566 (1975).
[16] T. Suzuki and H. Kim, J. Phys. Soc. Jpn. **40**, 1703 (1976).
[17] T. Suzuki, W. Skrotzki, and P. Haasen, Phys. Status Solidi B **103**, 763 (1981).
[18] J. W. Christian, in *Proceedings of the 2nd International Conference on Strength of Metals and Alloys* (American Society for Metals, Metals Park, Ohio, 1970), Vol. 1, p. 31.
[19] H. Saka, K. Noda, and T. Imura, Cryst. Lattice Defects **4**, 45 (1973).
[20] T. E. Mitchell, R. A. Foxall, and P. B. Hirsch, Philos. Mag. **8**, 1895 (1963).
[21] T. E. Mitchell, Philos. Mag. **17**, 1169 (1968).
[22] H. Suzuki, in *Dislocation Dynamics*, edited by A. R. Rosenfield, G. T. Hahn, A. L. Bement, and R. I. Jaffee (McGraw-Hill, New York, 1968), p. 679.
[23] V. Vitek, Cryst. Lattice Defects **5**, 1 (1974).
[24] H. O. K. Kirchner, in *Dislocations in Solids*, edited by H. Suzuki, T. Ninomiya, K. Sumino, and S. Takeuchi (University of Tokyo Press, Tokyo, 1985), p. 29.
[25] S. Takeuchi, in *Interatomic Potentials and Crystalline Defects*, edited by K. Lee (Metallurgical Society of AIME, New York, 1980), p. 201.
[26] F. Kroupa and V. Vitek, Can. J. Phys. **45**, 945 (1967).
[27] A. S. Argon and S. R. Maloof, Acta Metall. **14**, 1449 (1966).
[28] S. S. Lau and J. E. Dorn, Phys. Status Solidi A **2**, 825 (1970).
[29] K. Kitajima, Y. Aono, and E. Kuramoto, Scr. Metall. **15**, 919 (1981).
[30] S. Takeuchi, E. Kuramoto, and T. Suzuki, Acta Metall. **20**, 909 (1972).
[31] Y. Aono, E. Kuramoto, and K. Kitajima, in *Strength of Metals and Alloys*, edited by R. C. Gifkins (Pergamon, Oxford, 1982), p. 9.
[32] K. Kitajima, Y. Aono, H. Abe, and E. Kuramoto, in *Strength of Metals and Alloys*, edited by P. Haasen, V. Gerold, and G. Kostorz (Pergamon, Oxford, 1979), p. 965.
[33] M. S. Duesbery, in *Dislocations in Solids*, edited by F. R. N. Nabarro (North-Holland, Amsterdam, 1989), Vol. 8, p. 67.